ACS OMEGA

http://pubs.acs.org/journal/acsodf

Article

A Novel Polydopamine Grafted 3D MOF Nanocubes Mediated GR-5/GC DNAzyme Complex with Enhanced Fluorescence Emission Response toward Spontaneous Detection of Pb(II) and Ag(I) Ions

Pavadai Rajaji and Perumal Panneerselvam*

Cite This: https://dx.doi.org/10.1021/acsomega.0c03257

Read Online

ACCESS | Metrics & More | Article Recommendations

ABSTRACT: In this work, we have proposed a novel DNAzyme/MnCoPBAs-PDANCs complex-based fluorescence biosensor for subsequent detection of Pb^{2+} and Ag^{+} ions. The GR-5/GC-rich DNAzymes are strongly anchored or quenched on the surface of polydopamine hybridized 3D metal−organic framework MnCoPBAs-PDANCs by $\pi-\pi$ stacking interaction. Addition of Pb^{2+} ions has exhibited a catalytic inner cleavage of DNAzyme complex and disturbs to release shorter GC-rich sequence over the surface of MnCoPBAs-PDANCs complexes. Later on, addition of intercalating dye ThT interacts with free GC-rich substrate strand to form a G-quadruplex-ThT structure and thereby effectively enhanced the fluorescence intensity ("turn-on"). Interestingly, subsequent addition of Ag^{+} ions has an uncoiled GQ-ThT structure to provide a robust double-stranded DNA featuring C−Ag^{+}−C, which diminishes ("turn-off") the fluorescence intensity. This improved hybrid sensor exhibited a linear response in a concentration range of 3−9 nM for Pb^{2+}, while 4−20 nM for Ag^{+} ions with a lower detection limit of 1.6 and 4.2 nM, respectively. Further, the method was successfully implemented for the analysis of Pb^{2+} and Ag^{+} ions in real water samples with a good regaining and high efficacy for practical analysis.

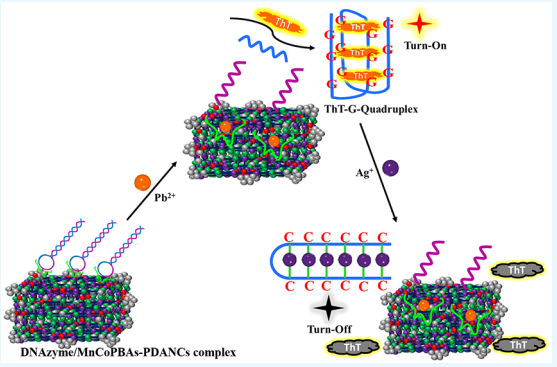

1. INTRODUCTION

Detection of hazardous heavy metal ions is one of the most inspiring tasks especially Pb^{2+} and Ag^{+} ions contamination has been considered as the furthermost toxic elements and as a mutual pollutant that holds severe risk for human health and the atmosphere. The Pb^{2+} and Ag^{+} ions are widespread water pollutants that are persistently toxic on bioaccumulation. A higher intake of Pb^{2+} ion induces toxic effects in a living organism through circulating in groundwater and soil.[1−4] Exposure to Pb^{2+} ions causes a variety of symptoms, particularly in children, such as muscle paralysis, irritability, anemia, and memory loss. An elevated level of Pb^{2+} ions has delayed the children's mental or physical development, and also it damages the cardiovascular, renal, and nervous systems. In our daily life, silver is an essential metal ion and it is commonly used for fields of electrical, photographic imaging, semiconductor, and biomedical research. In addition, silver poisoning causes a wide range of diseases, including internal organs, eyes, skins, and health effects in humans.[5−7] Consequently, developing an accurate quantitative system for the determination of Pb^{2+} and Ag^{+} ions is an urgent need.

Currently, several standard techniques have been existed to analyze the presence of Pb^{2+} and Ag^{+} ions, including XRF (X-ray fluorescence),[8] FAAS (flame atomic absorption spectrometry),[9] ICP-AES (inductively coupled plasma atomic emission spectroscopy),[10] AAS (atomic absorption spectrometry),[11] ICPMS (inductively coupled plasma mass spectrometry),[12] and SPME-HPLC (solid-phase micro-extraction coupled with high-performance liquid chromatography),[13] etc. However, these techniques often suffer with complex instrumentation such as sophisticated, time-consuming, low sensitivity, and tedious samplings preparation. The special features of electrochemical, colorimetric, and fluorometric biosensor have received an attention for quantitative analysis of heavy metal ions owing to their advantage such as cost-effective, as it's simple, fast, flexible, more effective, and highly sensitive with trace require amounts. At present, the development of DNAzyme-based fluorescent biosensor has emerged a new avenue in heavy metal sensing.

Recently, large number of nanomaterials has been established to support the fluorescent biosensor for the

Received: July 7, 2020
Accepted: September 8, 2020

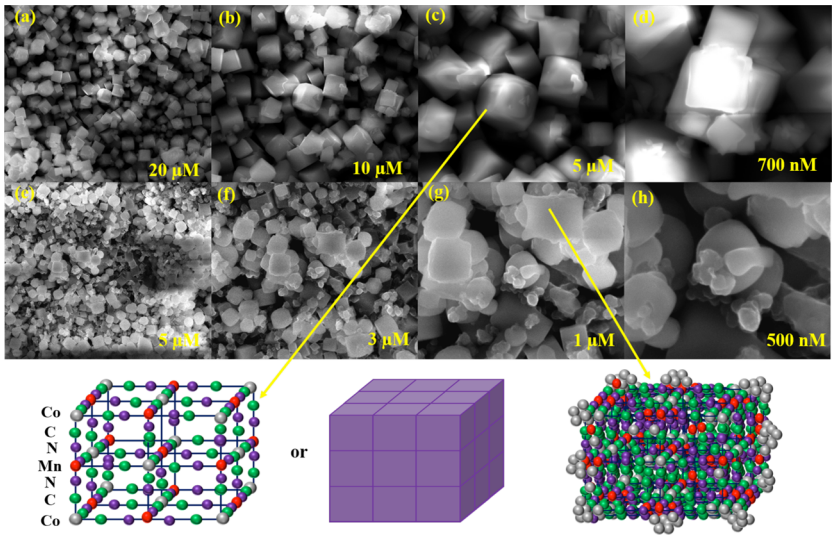

Figure 1. FE-SEM images of (a–d) MnCoPBAs-NCs and (e–h) MnCoPBAs-PDANCs.

detection of heavy metal ions. Particularly, the selection of nanomaterials, such as GO (graphene oxide), CNNSs (carbon nitride nanosheets), MoS_2 NSs (MoS_2 nanosheets), silica nanoparticles (Si-NPs), and swCNTs (single-walled carbon nanotubes)[14−18] are used as good quencher and also improves the signal to noise ratio of the aptamers. However, these nanomaterials have been successfully established for the fluorescence detection of metal ions, even though it is realized that the sensing medium quenches the fluorescence, it shows poor biodegradability, biocompatibility, and dispersion ability, and also the preparation of these nonmaterials was complicated. Consequently, it's provoked toward the substitution of new classes of nonmaterials.

In the past decade, MOF has been considered as promising candidates to explore attention owing to their varied morphologies, effective fluorescence quencher, uniformed structure, easily controllable size, good stability, and electrocatalytic activities, which enhance their applications in biomaterials.[19,20] The MOF is extensively used for the application of drug delivery, catalysis, separation, sensing, and detection of ascorbic acid, antibiotics, pesticide, hydrazine, and heavy metal ions.[21−26] Moreover, some drawbacks for this method lead to low detection ability, poor analytical performance, and weak GQ binding force between DNA strands and analytes.[27,28] The Prussian blue analogues (PBAs) of three-dimensional (3D) metal−organic frameworks (MOFs) were designated by the coordination of organic linker cyanide ligands with transition metal ions. In addition, polydopamine (PDA) has attracted the great attention owing to unique adhesive properties and synergistic interactions with nanomaterials. The surface functionality, good aqueous dispersibility, good biocompatibility, effective fluorescence quenching effect, and super hydrophobic surfaces of PDANPs exhibit specific $\pi-\pi$ stacking interactions to bind with DNA, thus enabling them as an ideal platform for biosensing applications.[29] The non-canonical four stands of a DNA GQ structure has intended from the DNA or RNA sequence are rich in guanine (G-rich).[30] The GQ-based sensor typically exhibits a high sensitivity for the detection of toxic metals ions.[31] Therefore, significant interest has been paid to the growth of MnCoPBAs-PDANCs and GR-5/GC-rich DNAzyme complex for fluorescence detection of metal ions.

In this work, we have reported the excellent quenching effect of MnCoPBAs-PDANCs for the spontaneous detection of Pb^{2+} and Ag^{+} ions. The synthesized MOF exhibits a large three-dimensional surface area with a specific molecular probe and good biocompatibility. The purposely designed GR-5/GC-rich specific DNAzyme functionalized onto MnCoPBAs-PDANCs and the fluorophore ThT was demonstrated in this biosensing platform. The subsequent detection of Pb^{2+} was feasible by catalytically cleaving the RNA sites of the substrate strand from DNAzyme/MnCoPBAs-PDANCs complex. So, there was enhanced fluorescence intensity because of the folding of a GQ structure during the addition of ThT-inducer. In addition, subsequent addition of Ag^{+} ion has uncoiled the GQ structure to form a C−Ag^{+}−C double strand DNA. The desorption of the fluorophore ThT has diminished in fluorescence intensity. Herein, the newly designed GR-5/GC-rich DNAzyme complex, and the proposed sensing mechanism have well supported the dual detection of Pb^{2+} and Ag^{+} ions in the environmental samples.

2. RESULT AND DISCUSSION

2.1. Characterization. The structure and morphology of the synthesized MnCoPBAs-NCs and MnCoPBAs-PDANCs were inspected by scanning electron microscopy (SEM). Figure 1a–d shows the image of MnCoPBAs-NCs that appears to be a well-defined cubic structure with an average particle size of 700 nm. Figure 1e–h exposes the monomer of dopamine that was successfully polymerized into the MnCoPBAs surface to form an irregular structure of MnCoPBAs-PDANCs. The addition of PDA has chelated with Mn^{2+} ion to form a PDA-Mn^{2+} intermediate (unstable) complex. To the above complex, an organic linker was added and thereby improved the stability of the complex. Finally, the polymerized dopamine complex MnCoPBAs-PDANCs was obtained. The typical HR-TEM microscopic images of the MnCoPBAs-PDANCs are shown in Figure 2. This image indicates that the dopamine monomer was polymerized on the outer surface of the MnCoPBAs-NCs.

Energy-dispersive X-ray spectroscopy (EDXS) shows (Figure 3a,b) that Mn, Co, C, and N elements are present in the MnCoPBAs-NCs. Additionally, the presence of oxygen element was noted in MnCoPBAs-PDANCs, which indicates

https://dx.doi.org/10.1021/acsomega.0c03257
ACS Omega XXXX, XXX, XXX−XXX

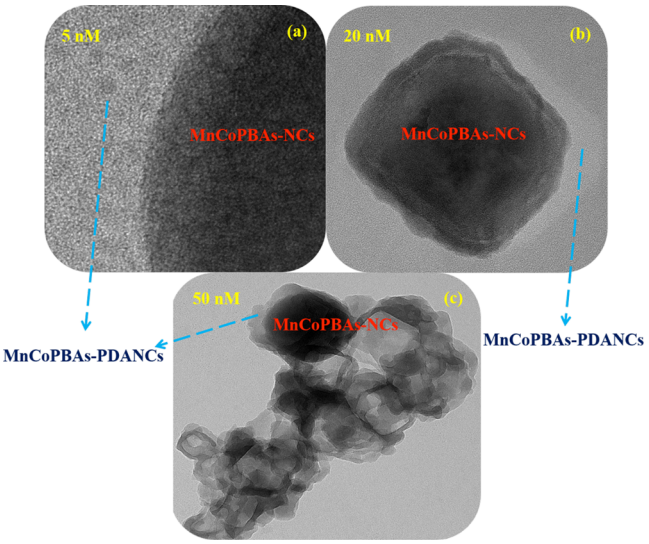

Figure 2. TEM images (a–c) are polymerized MnCoPBAs-PDANCs.

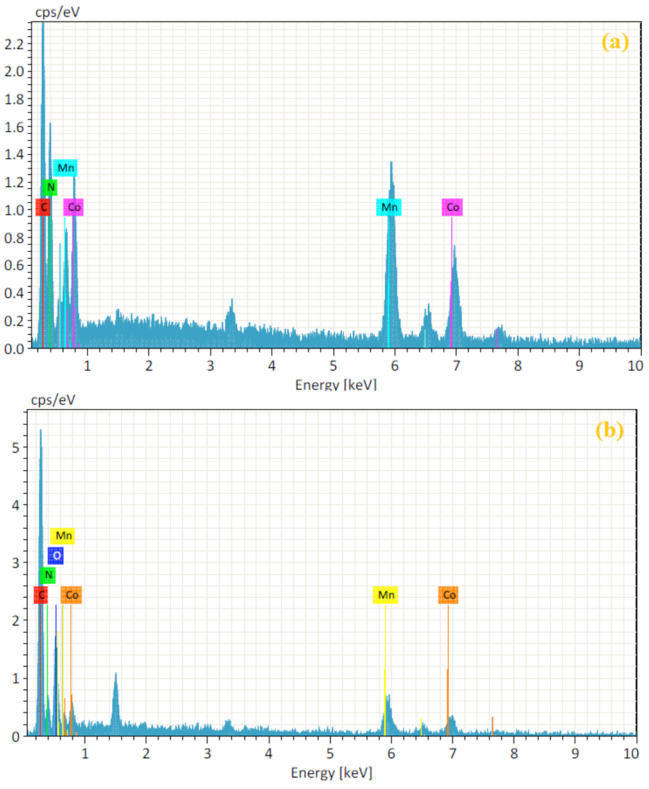

Figure 3. EDXS for (a) MnCoPBAs-NCs and (b) polymerized MnCoPBAs-PDANCs.

that dopamine monomer was completely polymerized into the surface of MnCoPBAs-NCs. The powder X-ray diffraction pattern studies were used to determine the crystalline nature of the prepared MnCoPBAs and MnCoPBAs-PDANCs. As shown in Figure 4, the XRD pattern of the two samples exhibits the diffraction peaks, which can be indexed well to the face-centered cubic phase (JCPDS 89-3735).[32] The spectra of these two samples were indexed with (200), (220), (400), (420), (422), (440), (600), (620), (640), and (642) planes. In contrast to MnCoPBAs-NCs, a minor broad peak centered at 21.4° was observed in the MnCoPBAs-PDANCs and that was corresponding to amorphous PDA in its pores. Finally, this

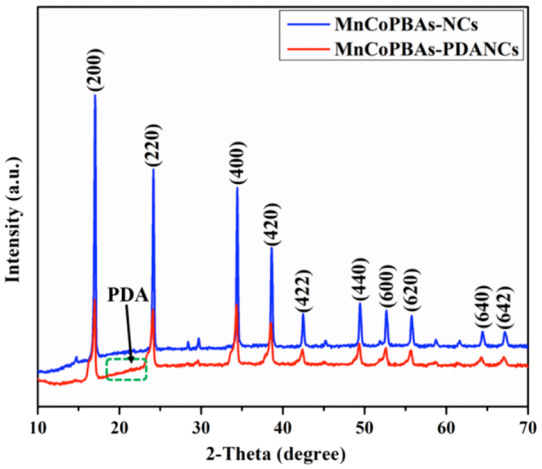

Figure 4. XRD spectra for MnCoPBAs-NCs and MnCoPBAs-PDANCs.

indicates that the dopamine monomers were polymerized into the pores and cubic surface of MnCoPBAs.

The FT-IR spectrum of MnCoPBAs and polymerized MnCoPBAs-PDANCs are shown in Figure 5, as follows: the

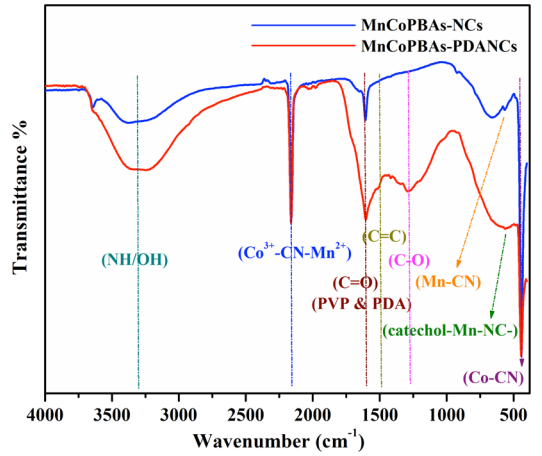

Figure 5. FT-IR spectra for MnCoPBAs-NCs and MnCoPBAs-PDANCs.

high-intensity peak located at 2162 cm^{-1} represents CN stretching in the Co^{3+}–CN–Mn^{2+} complex, and the metal cyanide Co–CN peak at 423 cm^{-1} was noted for both MnCoPBAs and MnCoPBAs-PDANCs. The MnCoPBAs were analyzed in the FT-IR region, Mn–CN and Co–CN exhibits a flexural absorption vibration at 563 and 423 cm^{-1}, respectively. In addition, specific absorption peaks located at 1604, 1505, and 1286 cm^{-1} assigned to the absorption of C═O, C═C, and C–O, respectively, in the aromatic rings of PDA exist in MnCoPBAs-PDANCs,[33,34] while the synthesized MnCoPBAs-NCs and MnCoPBAs-PDANCs attributed a C═O stretching peak at 1610 cm^{-1}. Furthermore N–H and –OH stretching vibration modes were observed around (3225–3350 cm^{-1}), respectively. The peak at 569 cm^{-1} evidences the catechol and cyanide group chelated with Mn^{2+} to form a polymerized product MnCoPBAs-PDANCs.

To further understand the elemental chemical state of the MnCoPBAs-PDANCs, the surface was examined by using XPS (Figure 6a–f). As shown in Figure 6a, the spectrum of

https://dx.doi.org/10.1021/acsomega.0c03257
ACS Omega XXXX, XXX, XXX–XXX

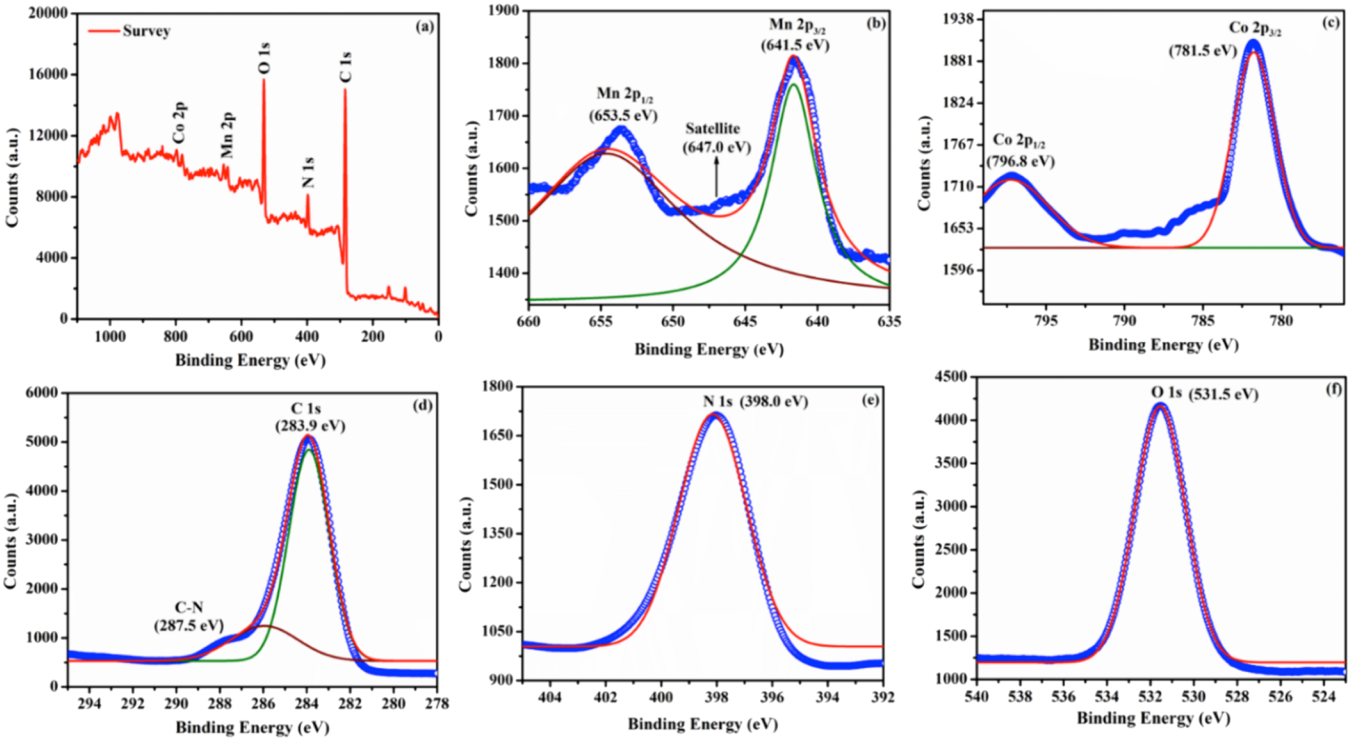

Figure 6. XPS spectrum of MnCoPBAs-PDANCs: (a) survey, (b) Mn 2p, (c) Co 2p, (d) C 1s, (e) N 1s, and (f) O 1s. The difference in the binding energy between Co $2p^{1/2}$ and Co $2p^{3/2}$ are corresponding to 15.3 eV, which revealed the coexistence of Co^{2+} and Co^{3+} species. Consequently, the C 1s high-resolution spectrum of the MnCoPBAs-PDANCs (d) could be curve-fitted with two peak components, having binding energies at 283.9 eV for the C−O species and 287.5 eV for the C−N species. Also, the N 1s spectra (e) had one peak at 398.0 eV, attributing the presence of C−N in the MnCoPBAs-PDANCs. As shown in (f), the peak at 531.5 eV was assigned to the lattice oxide oxygen of the metal oxides. The metal−oxygen (Mn−O) bond formation on the external surface is readily established by the XPS spectrum.[35,36]

MnCoPBAs-PDANCs confirmed the presence of Mn 2p, Co 2p, N 1s, O 1s, and C 1s peaks without any impurities. The MnCoPBAs-PDANCs (Figure 6b) show two typical peaks at 653.5 and 641.5 eV, which belong to Mn(II) $2p^{1/2}$ and Mn(II) $2p^{3/2}$ spin-orbit peaks, respectively. In addition, the Mn 2p scan of the MnCoPBAs-PDANCs that gave a distinct satellite "hump" around 647.0 eV was observed, further proving the presence of Mn^{2+}.[51] In the presence of Mn^{2+} with five unpaired 3d electrons creates MnCoPBAs-PDANCs, a virtuous candidate for the confirmation of the oxidation state of metal ions and its co-existence in other metal ions. As from the Co 2p, XPS spectra (Figure 6c), which exhibits the two distinct peaks centered at 796.8 and 781.5 eV, are assigned to Co $2p^{1/2}$ and Co $2p^{3/2}$ spin-orbit peaks, respectively.

2.2. Sensing Mechanism of Pb^{2+} and Ag^{+} Ions. The designed sensing mechanism was proposed for the MnCoPBAs-PDANCs-mediated GR-5/GC-rich DNAzyme complex-based biosensing probe for the highly sensitive detection of Pb^{2+} and Ag^{+} ions as depicted in Scheme 1. The substrate strand was developed by GC-rich sequences and it was hybridized with the DNAzyme strand, which leads to the formation of a DNAzyme-substrate complex having a hairpin-like single-strand DNA (ssDNA) stem-loop region. The GR-5/GC-rich DNAzyme is anchored on the surface of MnCoPBAs-PDANCs through hydrogen bonding and π-stacking interaction. This complex was diminishing the background signal because MnCoPBAs-PDANCs act as an effective quencher.

In addition of Pb^{2+} ions into the GR-5/GC-rich DNAzyme complex, it causes a catalytic inner cleavage and disturbs to release the shorter GC-rich sequence over the surface of

Scheme 1. Schematic Illustrations of the Fluorescence Detection of Pb^{2+} and Ag^{+} Ions by using the MnCoPBAs-PDANCs-Mediated GR-5/GC-Rich DNAzyme Complex

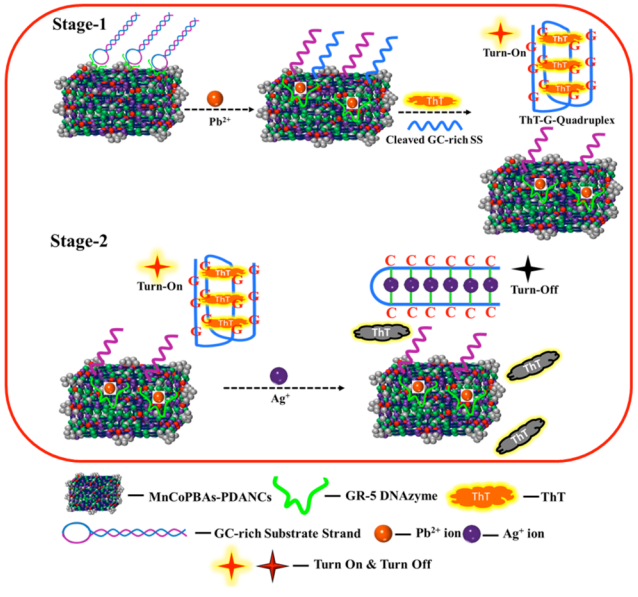

MnCoPBAs-PDANCs complexes. Then, an intercalating dye ThT was added, which made the freedom of GC-rich substrate strand (GC-rich SS), and folds to forming a G-quadruplex-ThT (GQ-ThT) structure, then efficiently enhanced the fluorescence intensity. In addition, further assay was employed for the subsequent detection of Ag^{+} ion using a GQ/ThT

https://dx.doi.org/10.1021/acsomega.0c03257
ACS Omega XXXX, XXX, XXX−XXX

system. Unbelievably, the fluorescence intensity was decreased by the addition of Ag^+ ion into the GQ/ThT system, because the GQ structure is uncoiled to form a duplex structure on releasing ThT dyes.

The formation of a C−Ag^+−C hairpin-like duplex structure was confirmed by the turn-off fluorescence intensity. As expected, this method plays as an off-sensor for Ag^+ ion. The fluorescence intensities were depicted in Figure 7, and it

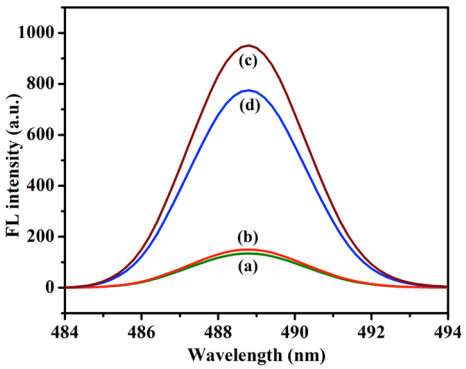

Figure 7. Changes of fluorescence spectra for (a) MnCoPBAs-PDANCs with GR-5/GC-rich DNAzyme complex, (b) MnCoPBAs-PDANCs with GR-5/GC-rich DNAzyme complex, Pb^{2+}, and (c) MnCoPBAs-PDANCs with GR-5/GC-rich DNAzyme complex, Pb^{2+}, ThT. (d) MnCoPBAs-PDANCs with GR-5/GC-rich DNAzyme complex, Pb^{2+}, ThT, and Ag^+.

demonstrates the probability of the planned MnCoPBAs-PDANCs/GR-5GC-rich DNAzyme structure induced fluorescent detection of Pb^{2+} and Ag^+ ion. As displayed in Figure 7a,b, Pb^{2+} ion reacts with MnCoPBAs-PDANCs-mediated GR-5/GC-rich DNAzyme complex structure resulting in a poor fluorescence signal. Figure 7c shows an increase in the fluorescence signal, which was observed when ThT was added to form the GQ structure. In turn, a decrease in the fluorescence signal was observed as shown in Figure 7d when the required concentration of Ag^+ ion was present in the same system.

2.3. Circular Dichroism Spectroscopy (CDS) Analysis. We further examined to confirm the sensing mechanism by using circular dichroism spectroscopy (CDS) where we have observed the conformational changes in GR-5 DS induced by Pb^{2+} and Ag^+ ions. Figure 8a shows the peak of GC-rich SS

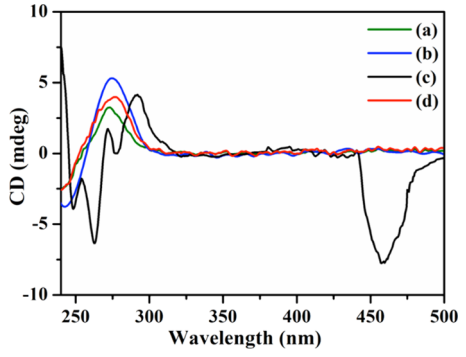

Figure 8. (a) GR-5 DS (6 μM); (b) GR-5 DS (6 μM) and SS (6 μM); (c) GR-5 DS (6 μM), SS (6 μM), Pb^{2+} (6 μM), and ThT (3 μM); and (d) GR-5 DS (6 μM), SS (6 μM), Pb^{2+} (6 μM), ThT (3 μM), and Ag^+ (6 μM).

with a concentration of 6 μM. A strong positive CDS peak at 274 nm and a negative peak at 243 nm were observed and these peaks correspond to the characteristics peak of single-strand DNA.

Moreover, the duplex structure (ssDNA stem-loop region) of the GR-5/GC-rich DNAzyme was developed by the 6 μM enzyme strand and 6 μM of the substrate strand. As a result, Figure 8b shows that the curve has dramatically increased the intensity of a positive CDS peak at 274 nm and a negative peak at 243 nm when compared to the curve (a). Expectedly, Figure 8c shows the unforeseen of a new peak. The addition of Pb^{2+} and ThT into the mixed GR-5/GC-rich DNAzyme leads to the formation of an antiparallel quadruplex structure, and it shows positive and negative peaks at 291 and 262 nm, respectively.[37] Upon addition of Pb^{2+} ion, the substrate strand was broken, and the released complexes were bounded to ThT. The strong negative peak at 457 nm shows that there was an interaction between the GQ and ThT. Finally, when the Ag^+ ion was added into the same system the CDS peak decreased as shown in Figure 8d due to the uncoiled GQ structure into a duplex structure (C−Ag^+−C).

2.4. Optimization of Experimental Condition. The optimization of the proposed sensor was evaluated with various influencing factors, including the amount of MnCoPBAs-PDANCs, GR-5 DS, the concentration of ThT, the effect of temperature, reaction time, and evolution of the signal-to-background ratio (S/B ratio). First, the fluorescence intensity of the sensing system was improved by varying the amount of MnCoPBAs-PDANCs. As shown in Figure 9a, the S/B ratio of the fluorescence intensity increased when the concentration of MnCoPBAs-PDANCs was 80 μg/mL. After gradually increasing the concentration of MnCoPBAs-PDANCs, the S/B ratio of the fluorescence intensity decreased due to excessive quenching effect and inhibited the release of a substrate strand from the surface of MnCoPBAs-PDANCs. Figure 9b illustrates the various concentrations of GR-5 DS. The concentration of the substrate strand is fixed as 50 nM since the S/B ratio is steadily increasing with an increase in the concentration of GR-5 DS. It can be observed that the concentration of GR-5 DS at 50 nM causes high cleavage efficiency and creates high signal. When the GR-5 DS concentration exceeds 50 nM the S/B ratio was decreased, then the internal cleavage effect of the GR-5 DS is not controlled. Therefore, 50 nM of GR-5 DS was chosen as the fixed concentration for further studies. As shown in Figure 9c, increase in the concentration of ThT dyes has rapidly increases the S/B ratio and reached a maximum range of 10 μM. Moreover, when the concentration of ThT is greater than 10 μM, it does not affect the sensing system. Subsequently, we performed the effect of reaction temperature at the range from 15 to 37 °C. Figure 9d shows that when we increase the temperature as well as the fluorescence intensity ($F-F_0$), the background noise was suppressed. However, the fluorescence signal was decreased sharply upon further increasing the temperature to 37 °C. As a result, increase in temperature above 37 °C causes the poor stability of the DNAzyme structure. Thus, 37 °C was working as the optimum reaction temperature for the subsequent experiments.

In addition, the effect of reaction time depends upon the catalytic cleavages of a DNAzyme, and therefore influences the formation of GQ. As displayed in Figure 9e, the fluorescent intensity of the DNAzyme complex decreased upon increasing time and reached saturation beyond 30 min. So, the optimal reaction time was chosen as 30 min for further experiments.

https://dx.doi.org/10.1021/acsomega.0c03257
ACS Omega XXXX, XXX, XXX−XXX

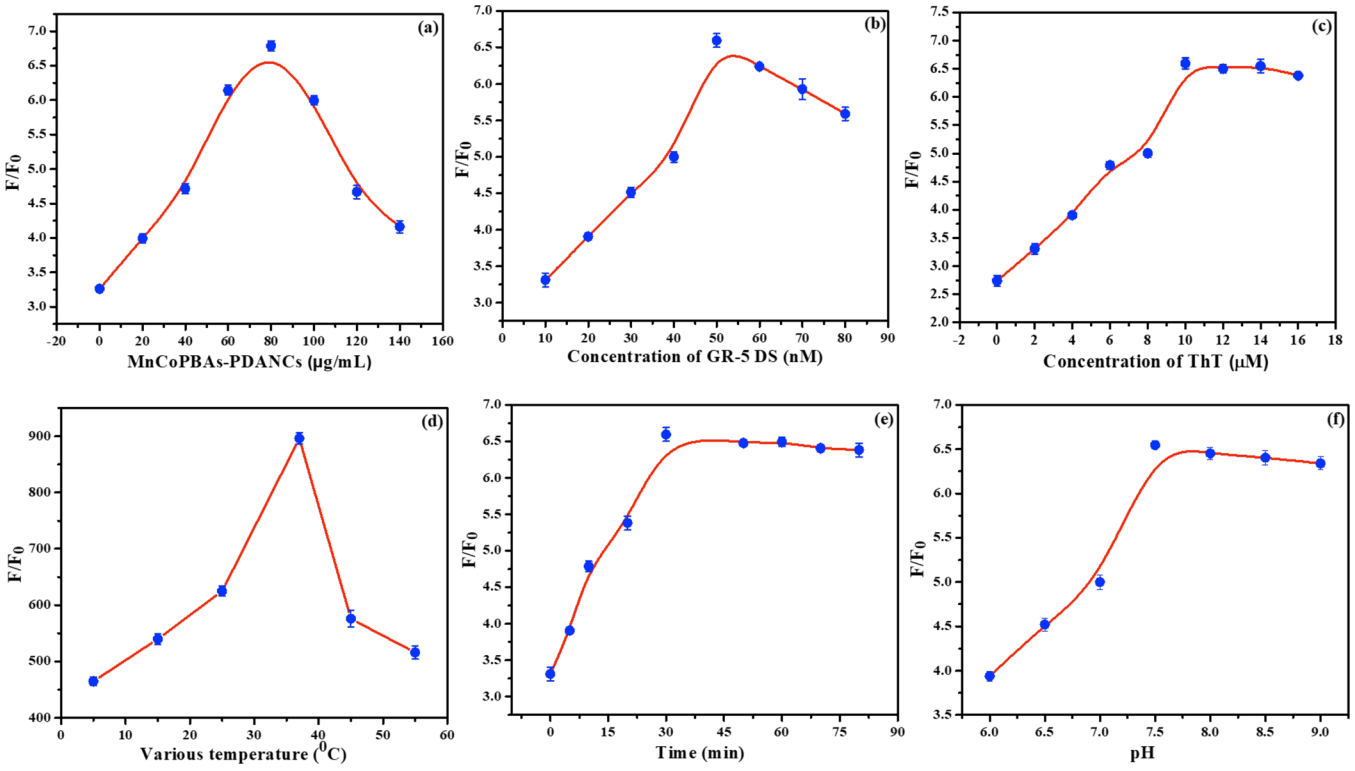

Figure 9. (a) Effect of various amounts for MnCoPBAs-PDANCs. The solution of 20 mM Tris (pH = 7.5) containing (SS (50 nM), GR-5 DS (50 nM)), Pb^{2+} (1 nM), and ThT (10 μM); (b) effect of concentration of GR-5 DS (50 nM).The solution of 20 mM Tris (pH = 7.5) containing MnCoPBAs-PDANCs (80 μg/mL), (SS (50 nM), Pb^{2+} (1 nM) and ThT (10 μM); and (c) effect of ThT(10 μM). The solution of 20 mM Tris (pH = 7.5) containing (SS (50 nM), GR-5 DS (50 nM), Pb^{2+} (1 nM) and MnCoPBAs-PDANCs (80 μg/mL), and (d–f) shows the effect of temperature, time, and pH: The solution of 20 mM Tris (pH = 7.5) containing MnCoPBAs-PDANCs (80 μg/mL), SS (50 nM), GR-5 DS (50 nM), and Pb^{2+} (1 nM) ThT (10 μM).

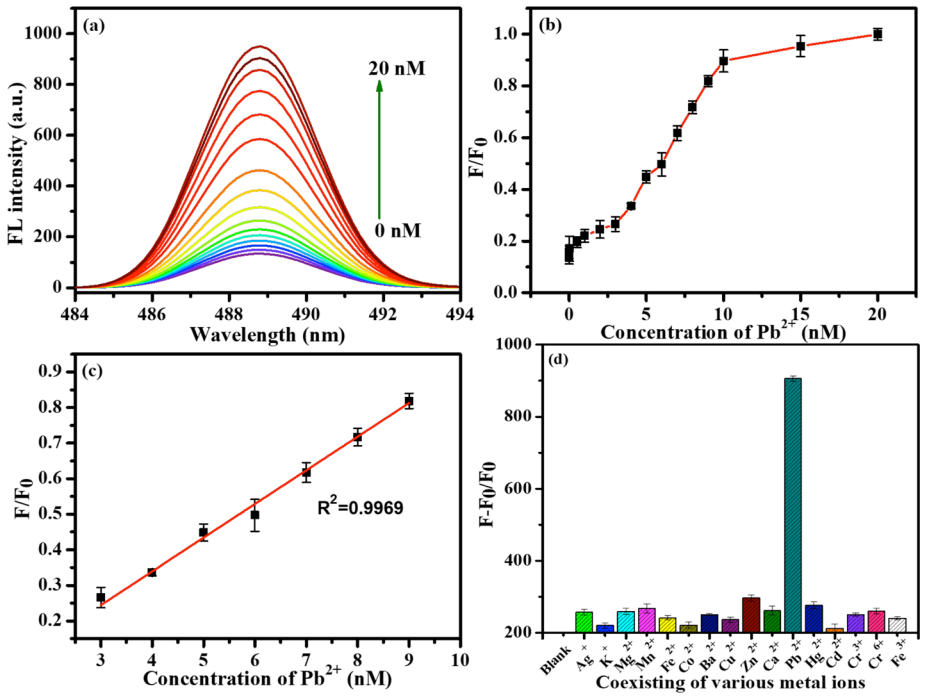

Figure 10. (a) Fluorescence spectra for Pb^{2+} MnCoPBAs-PDANCs (80 μg.mL^{-1}), SS (50 nM), GR-5 DS (50 nM), and ThT (10 μM) at various concentrations (0, 0.005, 0.01, 0.5, 1, 2, 3, 4, 5, 6, 7, 8, 9, 10, 15, and 20 nM) in 20 mM Tris (pH = 7.5) at 37 °C; (b) resolution of fluorescence against the Pb^{2+} concentrations; (c) linear relationship between fluorescence intensity and Pb^{2+} concentrations (3–9 nM); and (d) selectivity of Pb^{2+} (4 nM) and coexisting metal ions (8 nM). Error bars displayed the standard deviation for three individual tests.

https://dx.doi.org/10.1021/acsomega.0c03257
ACS Omega XXXX, XXX, XXX−XXX

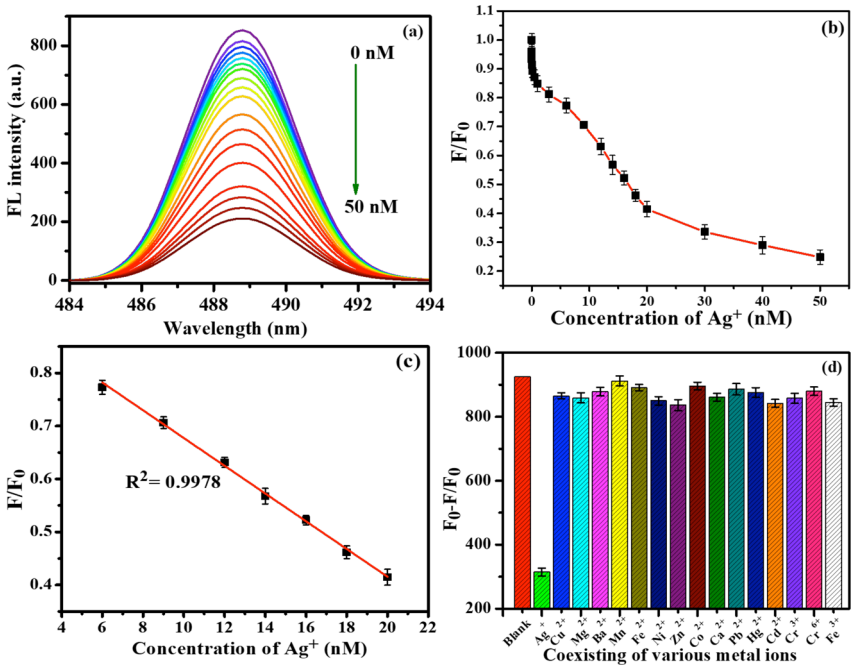

Figure 11. (a) Fluorescence spectra for Ag^{+}MnCoPBAs-PDANCs (80 μg.mL^{-1}), SS (50 nM), GR-5 DS (50 nM), ThT (10 μM), and Pb^{2+}(20 nM) at various concentrations (0, 0.005, 0.01, 0.05, 0.1, 0.5, 1, 3, 6, 9, 12, 14, 16, 18, 20, 30, 40, and 50 nM) in 20 mM Tris (pH = 7.5) at 37 °C; (b) resolution of fluorescence against the Pb^{2+} concentrations; (c) linear relationship between fluorescence intensity and Pb^{2+} concentrations (4−20 nM); and (d) Ag^{+} (4 nM) selectivity and coexisting metal ions (8 nM). For three individual tests, error bars display the standard deviation.

2.5. Sensitivity and Selectivity of Pb^{2+} and Ag^{+} Ions.

The sensitivity response of the biosensor was investigated for the dual detection of Pb^{2+} and Ag^{+} ions. As revealed in Figure 10a,b, increasing the concentration of Pb^{2+} ion over the range of 3 to 9 nM, shows a significant increase in fluorescence intensity. It was recognized that the conformational changes of GR-5/GC-rich DNAzyme complex and the shorter GC-rich sequence were released from the surface of MnCoPBAs-PDANCs. Further, ThT was added and allowed to react with shorter GC-rich sequence to form a quadruplex formation. This results in the enhancement of fluorescent intensity with an excitation and emission wavelengths of 425 and 489 nm, respectively. The limit of detection was estimated to be 1.6 nM using 3σ/slop rules. Then, R^2 = 0.9969 value exhibit the linear correlation coefficient between the concentration of Pb^{2+} ion versus fluorescence intensity, as shown in Figure 10c.

The selectivity study of this sensing system was performed to identify the interference of other metal ions. The other competitive metal (M^{2+} and M^{+}) ions such as Ba, Mg, Ca, Zn, Cd, Mg, Cd, Cu, Co, Fe, Mn, K, and Ag were introduced into the GR-5/GC-rich DNAzyme complex. It can be seen from Figure 10d that other interfering metal ions does not cause any significant changes in fluorescent intensity. The selectivity toward Pb^{2+} ion was confirmed by fluorescence enhancing effect, due the selective cleaving of RNA site from the substrate strand by Pb^{2+} ion.[38] In addition, the specific selectivity of another metal ion (Ag^{+}) by using a specific sequence of GC-rich substrate strand. This process was observed in the MnCoPBAs-PDANCs-mediated GR-5/GC-richDNAzyme@Pb^{2+}@ThT@GQ system.

Furthermore, subsequent addition of Ag^{+} ion has effectively turned-off the fluorescence intensity. Figure 11a,b shows that a continuous increase in the concentration of Ag^{+} ion has a gradual decrease in the fluorescence intensity. Figure 11c shows a perfect linear relationship (R^2 = 0.9978) detected in the range of 6 to 20 nM and the detection limit is 4.2 nM, which was determined by using the 3σ/slop rule. The DNAzyme/MnCoPBAs-PDANCs complex-based fluorescent biosensor had superior sensitivity in the detection of Pb^{2+} and Ag^{+} ions. The advantages of the present sensing system were compared with the previously reported biosensors as shown in Tables 1 and 2. Our sensing system has exhibited a high sensitivity for dual detection of Pb^{2+} and Ag^{+} ions.

Subsequently, Ag^{+} ion was added into this complex, it produced the duplex structure. The structure of GQ/ThT has uncoiled to release the ThT dye that leads to a decrease in fluorescence intensity. However, sensing assay performed for co-existing metal ions, showed no interfere as shown from

Table 1. Comparison of Various Nanomaterials Used to Determine Pb^{2+} Ions[a]

materials	method	LOD	real sample	ref
guadruplex/GO/AO	FLS	3 nM	lake and tap water	39
GR-5 DS	FLS	3 nM	river water	40
Ag NCs/DNA	FLS	3 nM	tap and lake water	41
AuNPs/DNAzyme	FLS	5 nM	tap water	42
L-DNAzyme	FLS	3 nM	river water	43
DNA-catalyzed porphyrin metalation	FLS	23.5 nM	not mentioned	44
aptamer-functionalized (UCNPs)	FLS	5.7 nM	tea and waste water	45
MnCoPBAs-PDANCs-mediated GR-5/GC-rich DNAzyme	FLS	1.6 nM	tap and lake water	this work

[a]FLS-Fluorescence spectroscopy, GO-graphene oxide, and UCNPs-upconversion nanoparticles.

https://dx.doi.org/10.1021/acsomega.0c03257
ACS Omega XXXX, XXX, XXX−XXX

Table 2. Comparison of Various Nanomaterials Used to Determine Ag^+ Ion[a]

materials	method	LOD	real sample	ref
2-Aminopurine/DNA	FLS	3.0 nM	lake water	46
SYBER Green	FLS	4.3 nM	not reported	47
GO	FLS	5.0 nM	river water	14
L-Aspartic Acid Capped CdS QDs	FLS	30 nM	drinking water	48
MnO_2 nanosheet/DNA	FLS	9.1 nM	tap and lake water	49
MnCoPBAs-PDANCs-mediated GR-5/GC-rich DNAzyme	FLS	4.2 nM	tap and lake water	this work

[a]FLS-Fluorescence spectroscopy, QDs-quantum dots.

Figure 11d. Thus, the proposed biosensor was successfully examined for the dual detection of Pb^{2+} and Ag^+ ions.

2.6. The Practical Utility of Real Water Sample (RWS). The GR-5/GC-rich DNAzyme/MnCoPBAs-PDANCs were investigated for the practical applicability by detecting Pb^{2+} and Ag^+ ions in the environmental water samples. The tap and lake water were collected near SRM IST campus, Tamilnadu, India and then filtered to eliminate insoluble impurities. This sensing system was spiked with different concentrations of Pb^{2+} and Ag^+ ions, and the experimental results are reported in Table 3. The satisfactory recovery of Pb^{2+} and Ag^+ ions were verified in the range from 96.05 to 105.05% and 96.05 to 105.05%, respectively. Hence the fluorescent biosensing method was successfully executed for environmental water samples with satisfactory accuracy and it is suitable for practical use.

3. CONCLUSIONS

In summary, we have prepared self-assembled polydopamine grafted 3D MOF nanocubes (MnCoPBAs-PDANCs)-GR-5/GC-rich DNAzyme complex for subsequent detection of Pb^{2+} and Ag^+ ions. Of the challenging note, the tailored 3D MnCoPBAs-PDANCs has effectively quenched with GR-5/GC-rich DNAzyme, it benefits the successful development of sensors in this modification route. The Pb^{2+} ions selectively cleave the substrate strand at the MOF nanocubes surface to release the shorter GC-rich sequence, meanwhile the thioflavin-T (ThT) fluorescent dye induced G-quadruplex system assisted signal amplification (turn-on). Subsequently, C−Ag^+−C chelation releases the ThT, resulting in diminishing of fluorescence intensity (turn-off). This sensing method has achieved the detection limit of 1.6 and 4.2 nM for Pb^{2+} and Ag^+ ions correspondingly, which was noticeably superior to that of similar sensing assays. Overall, this approach shows simple, reliable, and outstanding analytical performance for the selective and sensitive detection of Pb^{2+} and Ag^+ ions in real water samples, which may also probably applied for the sensing of environmental and biological applications.

4. EXPERIMENTAL SECTION

4.1. Materials and Instruments. Dopamine, thioflavin-T(3,6-dimethyl-2-(4-methylaminophenyl)benzothiazolium cation), potassium hexacyanocobaltate(III) ($K_3[Co(CN)_6]$), manganese acetate ($Mn(COO)_2.4H_2O$), tris(hydroxymethyl)-aminomethane, and metal nitrates, metal halides such as lead nitrate, mercury nitrate, silver nitrate, calcium chloride, nickel chloride, potassium acetate, cobalt chloride, copper chloride, cadmium chloride, ferric chloride, magnesium chloride, zinc chloride, barium chloride, ferrous chloride, manganese chloride, and other standard chemicals were purchased from the Sigma-Aldrich and SRL chemicals. The buffer is prepared from Tris (20 mM), KCl (200 mM), and $MgCl_2$ (10 mM) (pH = 7.5). The 10 mM ThT stock solution was prepared in Milli-Q water and stored at 4 °C under dark condition. All these chemical reagents were analytical grade or reagent grade and directly used as received without further purification. The enzyme strand and substrate strand DNA were obtained from Allied Scientific Products (Kolkata, India) and their GR-5 DNAzyme probes are given as follows

GR-5 DS: (5′-CCAAAGTGCTCCGAGCCGGTC-GAAGCTCTCCC-3′)

GC-rich for SS:

(5′-TAGGGCCCCGGGCCCCCCGGGCCCCGGGA-GAGCTrAGGCACTTTGGGTAGGG-3′)

The MnCoPBAs-NCs and MnCoPBAs-PDANCs morphologies were observed by using the FEI Quanta FEG 200 scanning electron microscope (SEM) at an accelerated voltage of 20 kV. The transmission electron microscopic (TEM) images of the MnCoPBAs-NCs were analyzed at an operating voltage of 2000 kV on a JEOL/JEM-2100. The crystalline nature of the MnCoPBAs-NCs and MnCoPBAs-PDANCs were evaluated at Cu Kα radiation (α = 1,54 Å) using X-ray diffraction (XRD) analysis source (PAN analytical (40 kV) X'pert power diffractometer). An Agilent Technology FT-IR spectrometer (USA) was used to find the Fourier transform infrared (FT-IR) spectra. A fluoromax-4 spectrofluorometer model (HORIBA Scientific, France) has been used to record fluorescence and emission spectra with a 10 nm slit width for both excitation and emission. For the samples, excitation and emission wavelengths were measured at 425 nm and 489 nm, respectively. Circular dichroism (CD) measurements had been carried out via the JASCO J-815 spectrometer (JASCO International Co. Ltd., Japan). These spectra have been measured at a wavelength range of 200−500 nm using a 1.0

Table 3. Determination of Persistence for Pb^{2+} and Ag^+ Ions in RWS Using the Proposed Strategy

samples	spiked (nM)	detected ± SD		recovery (%)	
		Pb^{2+}	Ag^+	Pb^{2+}	Ag^+
tap water	2	$2.101^x \pm 0.56^y$	$1.921^x \pm 0.56^y$	105.05	96.05
	4	$4.203^x \pm 0.42^y$	$4.123^x \pm 0.65^y$	105.07	105.05
	6	$6.257^x \pm 1.31^y$	$6.101^x \pm 2.21^y$	104.28	101.6
lake water	2	$2.102^x \pm 0.64^y$	$2.012^x \pm 0.75^y$	105.1	100.6
	4	$3.972^x \pm 0.74^y$	$3.972^x \pm 0.11^y$	96.05	96.05
	6	$6.021^x \pm 1.17^y$	$6.032^x \pm 0.29^y$	100.35	100.5

https://dx.doi.org/10.1021/acsomega.0c03257
ACS Omega XXXX, XXX, XXX−XXX

mm path length quartz cuvette. Analysis of X-ray photoelectron spectroscopy (XPS) was determined on an ESCALAB MK II X-ray photoelectron spectrometer using Mg as the source of excitation.

4.2. Synthesis of 3D MnCoPBAs-NCs. The MnCoPBAs-NCs were synthesized through a co-precipitation reaction technique according to the literature.[50] Briefly, 12.9 mg of $Mn(CH_3COO)_2.4H_2O$ and 0.3 g of PVP (K-30) were first dissolved in 40 mL of aqueous solution and then magnetic stirring was continued for 30 min. Then, the reaction mixture was well dispersed using deionized water and ethanol (v/v = 1:3), and the stirring was continued to form a transparent solution. Thereafter, 10 mL of $K_3[Co(CN)_6]$ (13.2 mg) solution was added dropwise into the above solution and stirred for 30 min and then the reaction was continued for 12 h. Finally, the precipitate was filtered, washed numerous times with ethanol and water. The obtained product was dried at room temperature for 6 h.

4.3. Synthesis of 3D MnCoPBAs-PDANCs. The 3D MnCoPBAs-polydopamine nanocubes (MnCoPBAs-PDANCs) were synthesized by following the modified procedure.[51] Typically, 0.03 M $Mn(CH_3COO)_2.4H_2O$ and 0.06 M dopamine were first dissolved using 40 mL of deionized water and ethanol (1:3) solution. The suspension was constantly stirred for sufficient time. The coordination polymer of dopamine chelated with Mn^{2+} was obtained as the product. The schematic representation of the above product is shown in scheme 2. Consequently, 0.04 M $K_3[Co(CN)_6]$ was

Scheme 2. Schematic Representation of the Synthesis of MnCoPBAs-PDANCs

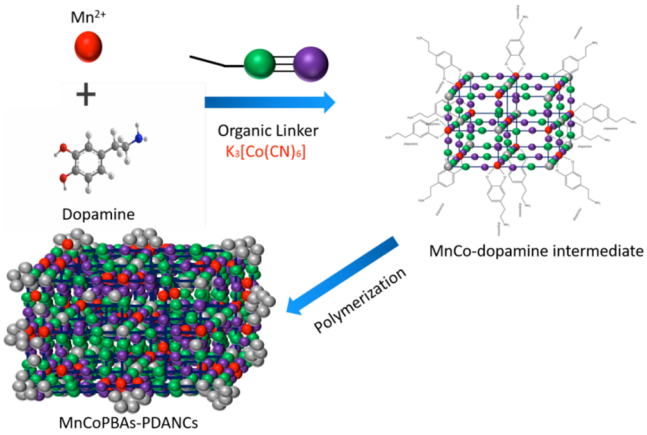

added dropwise to the above mixture under vigorous stirring. The suspension was stirred for 24 h at room temperature to complete the polymerization. Finally, the black precipitate is obtained by centrifugal separation and washed with absolute ethanol not less than five times.

4.4. Detection of Pb^{2+} and Ag^{+} Sensor. The analytical technique for dual detection of Pb^{2+} and Ag^{+} biosensor was explored by the desired concentration of GR-5 DNAzyme strand (10 μL of 3 μM) and GC-rich SS (5 μL of 3 μM) were hybridized in a buffer solution (20 mM Tris, 200 mM KCl, and 10 mM $MgCl_2$; pH = 7.5) for 30 min at 37 °C. The Pb^{2+} sensor, 10 μL of a GR-5 DNAzyme strand (GR-5 DS), 200 μL of a buffer solution (50 mM of HEPES, 50 mM NaCl, and 5 mM $MgCl_2$; pH = 7.4), and 80 μg/mL MnCoPBAs-PDANCs were consecutively added into a plastic micro centrifuge tube. After 30 min of reaction, the solution was shifted into a cuvette. Then, the freshly prepared 10 μL of Pb^{2+} ion was added in a concentration range of 0 to 20 nM and then nurtured for 40 min. Further, 60 μL of 10 μM ThT was added and allowed to react for 30 min at 37 °C to form the quadruplex formation of the sensing system. The enhancement in fluorescent intensity of the solution was measured at excitation and emission wavelengths of 425 and 489 nm, respectively. The subsequent detection of the Ag^{+} sensor was performed in the above sensing system by adding 10 μL Ag^{+} ions in a concentration range of 0 to 50 nM. The diminished in fluorescent intensity with excitation and emission wavelengths at 425 and 489 nm, respectively, were observed from fluorescence spectra.

4.5. Investigation of Real Water Samples (RWS). The synthesized MnCoPBAs-PDANCs mediated GR-5/GC-rich DNAzyme complex-based biosensor was investigated for the real water samples analysis. The water samples were collected from the SRM Institute campus, Chennai, India. First, insoluble impurities from water samples were removed by using a 0.22 μM membrane filter. Consequently, the various concentrations of (2, 4, and 6 nM) Pb^{2+} and Ag^{+} ions were spiked in RWS, and the fluorescence studies of Pb^{2+} and Ag^{+} ions we performed by following the above detection procedure.

AUTHOR INFORMATION

Corresponding Author

Perumal Panneerselvam − *Department of Chemistry, SRM Institute of Science and Technology, Kattankulathur 603 203, Tamil Nadu, India;* orcid.org/0000-0003-2647-6835; Phone: +91 9688538842; Email: panneerp1@srmist.edu.in, panneerchem82@gmail.com

Author

Pavadai Rajaji − *Department of Chemistry, SRM Institute of Science and Technology, Kattankulathur 603 203, Tamil Nadu, India*

Complete contact information is available at: https://pubs.acs.org/10.1021/acsomega.0c03257

Notes

The authors declare no competing financial interest.

ACKNOWLEDGMENTS

Authors acknowledge the financial support from the Department of Chemistry, SRM Institute of Science and Technology, Tamil Nadu-603 203, India.

REFERENCES

(1) Alvarez, A.; Saez, J. M.; Costa, J. S.; Colin, V. L.; Fuentes, M. S.; Cuozzo, S. A.; Benimeli, C. S.; Polti, M. A.; Amoroso, M. J. Actinobacteria: current research and perspectives for bioremediation of pesticides and heavy metals. *Chemosphere* **2017**, *166*, 41−62.

(2) Flora, S. J. S. Metal poisoning: threat and management. *Al Ameen J. Med. Sci.* **2009**, *2*, 4−26.

(3) Ratte, H. T. Bioaccumulation and toxicity of silver compounds: a review. *Environ. Toxicol. Chem.* **1999**, *18*, 89−108.

(4) Barriada, J. L.; Tappin, A. D.; Evans, E. H.; Achterberg, E. P. Dissolved silver measurements in seawater. *TrAC, Trends Anal. Chem.* **2007**, *26*, 809−817.

(5) Zhu, G.; Zhang, C.-y. Functional nucleic acid-based sensors for heavy metal ion assays. *Analyst* **2014**, *139*, 6326−6342.

(6) Ramachandran, R.; Chen, T.-W.; Chen, S.-M.; Baskar, T.; Kannan, R.; Elumalai, P.; Raja, P.; Jeyapragasam, T.; Dinakaran, K. A

https://dx.doi.org/10.1021/acsomega.0c03257
ACS Omega XXXX, XXX, XXX−XXX

review of the advanced developments of electrochemical sensors for the detection of toxic and bioactive molecules. *Inorg. Chem. Front.* **2019**, *6*, 3418−3439.
(7) Kleinke, K.; Saran, R.; Liu, J. Label-free Ag^{+} detection by enhancing DNA sensitized Tb^{3+} luminescence. *Sensors* **2016**, *16*, 1370.
(8) Van Meel, K.; Smekens, A.; Behets, M.; Kazandjian, P.; Van Grieken, R. Determination of platinum, palladium, and rhodium in automotive catalysts using high-energy secondary target X-ray fluorescence spectrometry. *Anal. Chem.* **2007**, *79*, 6383−6389.
(9) Ghaedi, M.; Shokrollahi, A.; Niknam, K.; Niknam, E.; Najibi, A.; Soylak, M. Cloud point extraction and flame atomic absorption spectrometric determination of cadmium (II), lead (II), palladium (II) and silver (I) in environmental samples. *J. Hazard. Mater.* **2009**, *168*, 1022−1027.
(10) Ganjali, M. R.; Daftari, A.; Hajiagha-Babaei, L.; Badiei, A.; Saberyan, K.; Ziarani, G. M.; Moghimi, A. Pico level monitoring of silver with modified hexagonal mesoporous compound (MCM-41) and inductively coupled plasma atomic emission spectrometry. *Water, Air, Soil Pollut.* **2006**, *173*, 71−80.
(11) Thulasidas, S. K.; Kulkarni, M. J.; Porwal, N. K.; Page, A. G.; Sastry, M. D. Direct determination of beryllium, cadmium, lithium, lead and silver in thorium nitrate solution by electrothermal atomization atomic absorption spectrometry. *Anal. Lett.* **1988**, *21*, 265−278.
(12) Welch, C. J.; Albaneze-Walker, J.; Leonard, W. R.; Biba, M.; DaSilva, J.; Henderson, D.; Laing, B.; Mathre, D. J.; Spencer, S.; Bu, X.; Wang, T. Adsorbent screening for metal impurity removal in pharmaceutical process research. *Org. Process Res. Dev.* **2005**, *9*, 198−205.
(13) Königsberger, K.; Chen, G.-P.; Wu, R. R.; Girgis, M. J.; Prasad, K.; Repič, O.; Blacklock, T. J. A practical synthesis of 6-[2-(2, 5-dimethoxyphenyl) ethyl]-4-ethylquinazoline and the art of removing palladium from the products of Pd-catalyzed reactions. *Org. Proc. Res. Dev.* **2003**, *7*, 733−742.
(14) Wen, Y.; Xing, F.; He, S.; Song, S.; Wang, L.; Long, Y.; Li, D.; Fan, C. A graphene-based fluorescent nanoprobe for silver (I) ions detection by using graphene oxide and a silver-specific oligonucleotide. *Chem. Commun.* **2010**, *46*, 2596−2598.
(15) Wang, Q.; Wang, W.; Lei, J.; Xu, N.; Gao, F.; Ju, H. Fluorescence quenching of carbon nitride nanosheet through its interaction with DNA for versatile fluorescence sensing. *Anal. Chem.* **2013**, *85*, 12182−12188.
(16) Mao, K.; Wu, Z.; Chen, Y.; Zhou, X.; Shen, A.; Hu, J. A novel biosensor based on single-layer MoS2 nanosheets for detection of Ag +. *Talanta* **2015**, *132*, 658−663.
(17) Yang, S.; Liu, M.; Deng, F.; Mao, L.; Yuan, Y.; Huang, H.; Chen, J.; Liu, L.; Zhang, X.; Wei, Y. Biomimetic modification of silica nanoparticles for highly sensitive and ultrafast detection of DNA and Ag^{+} ions. *Appl. Surf. Sci.* **2020**, *510*, 145421.
(18) Niu, S. Y.; Li, Q. Y.; Ren, R.; Hu, K. C. DNA/single-walled carbon nanotubes-based fluorescence detection of Hg^{2+}. *Anal. Lett.* **2010**, *43*, 2432−2439.
(19) Ravikumar, A.; Panneerselvam, P.; Morad, N. Metal−polydopamine framework as an effective fluorescent quencher for highly sensitive detection of Hg^{2+} and Ag^{+} ions through exonuclease III activity. *ACS Appl. Mater. Interfaces* **2018**, *10*, 20550−20558.
(20) Chen, W.; Gao, G.; Jin, Y.; Deng, C. A facile biosensor for Aβ40O based on fluorescence quenching of prussian blue nanoparticles. *Talanta* **2020**, *216*, 120930.
(21) Zakaria, M. B.; Chikyow, T. Recent advances in Prussian blue and Prussian blue analogues: synthesis and thermal treatments. *Coord. Chem. Rev.* **2017**, *352*, 328−345.
(22) Rama, M. J. R.; Medina, A. R.; Díaz, A. M. A Prussian blue-based flow-through renewable surface optosensor for analysis of ascorbic acid. *Microchem. J.* **2004**, *78*, 157−162.
(23) Zhao, Y.; Wei, Q.; Xu, C.; Li, H.; Wu, D.; Cai, Y.; Mao, K.; Cui, Z.; Du, B. Label-free electrochemical immunosensor for sensitive detection of kanamycin. *Sens. Actuators, B* **2011**, *155*, 618−625.
(24) Zhao, H.; Ji, X.; Wang, B.; Wang, N.; Li, X.; Ni, R.; Ren, J. An ultra-sensitive acetylcholinesterase biosensor based on reduced graphene oxide-Au nanoparticles-β-cyclodextrin/Prussian blue-chitosan nanocomposites for organophosphorus pesticides detection. *Biosens. Bioelectron.* **2015**, *65*, 23−30.
(25) Zhao, J.; Yue, P.; Tricard, S.; Pang, T.; Yang, Y.; Fang, J. Prussian blue (PB)/carbon nanopolyhedra/polypyrrole composite as electrode: a high performance sensor to detect hydrazine with long linear range. *Sens. Actuators, B* **2017**, *251*, 706−712.
(26) Li, X.; Liu, Y.; Zhang, C.; Wen, T.; Zhuang, L.; Wang, X.; Song, G.; Chen, D.; Ai, Y.; Hayat, T.; Wang, X. Porous Fe_2O_3 microcubes derived from metal organic frameworks for efficient elimination of organic pollutants and heavy metal ions. *Chem. Eng. J.* **2018**, *336*, 241−252.
(27) Wang, M.; Yang, L.; Hu, B.; Liu, J.; He, L.; Jia, Q.; Song, Y.; Zhang, Z. Bimetallic NiFe oxide structures derived from hollow NiFe Prussian blue nanobox for label-free electrochemical biosensing adenosine triphosphate. *Biosens. Bioelectron.* **2018**, *113*, 16−24.
(28) Gu, C.; Yang, L.; Wang, M.; Zhou, N.; He, L.; Zhang, Z.; Du, M. A bimetallic (Cu-Co) Prussian Blue analogue loaded with gold nanoparticles for impedimetric aptasensing of ochratoxin a. *Microchim. Acta* **2019**, *186*, 343.
(29) Cheng, W.; Zeng, X.; Chen, H.; Li, Z.; Zeng, W.; Mei, L.; Zhao, Y. Versatile polydopamine platforms: synthesis and promising applications for surface modification and advanced nanomedicine. *ACS Nano* **2019**, *13*, 8537−8565.
(30) Yang, D. G-Quadruplex DNA and RNA. In *G-Quadruplex Nucleic Acids*; Humana: New York, NY, 2019, 1−24.
(31) Ge, J.; Li, X. P.; Jiang, J. H.; Yu, R. Q. A highly sensitive label-free sensor for Mercury ion (Hg^{2+}) by inhibiting thioflavin T as DNA G-quadruplexes fluorescent inducer. *Talanta* **2014**, *122*, 85−90.
(32) Pang, H.; Wang, W.; Yan, Z.; Zhang, H.; Li, X.; Chen, J.; Zhang, J.; Zhang, B. Porous $Mn_3[Co(CN)_6]_2.nH_2O$ nanocubes as a rapid organic dyes adsorption material. *RSC Adv.* **2012**, *2*, 9614−9618.
(33) Lin, X.; Cao, Y.; Li, J.; Zheng, D.; Lan, S.; Xue, Y.; Yu, F.; Wu, M.; Zhu, X. Folic acid-modified Prussian blue/polydopamine nanoparticles as an MRI agent for use in targeted chemo/photothermal therapy. *Biomater. Sci.* **2019**, *7*, 2996−3006.
(34) Parnell, C. M.; Chhetri, B.; Brandt, A.; Watanabe, F.; Nima, Z. A.; Mudalige, T. K.; Biris, A. S.; Ghosh, A. Polydopamine-coated manganese complex/graphene nanocomposite for enhanced electrocatalytic activity towards oxygen reduction. *Sci. Rep.* **2016**, *6*, 31415.
(35) Carvalho, C. L. C.; Silva, A. T. B.; Luz, R. A. S.; Castro, G. M. B.; da Luz Lima, C.; Mastelaro, V. R.; da Silva, R. R.; Oliveira, O. N., Jr.; Cantanhâde, W. Development of $Co_3[Co(CN)_6]_2/Fe_3O_4$ bifunctional nanocomposite for clinical sensor applications. *ACS Appl. Nano Mater.* **2018**, *1*, 4283−4293.
(36) Zhang, L.; Shi, L.; Huang, L.; Zhang, J.; Gao, R.; Zhang, D. Rational Design of High-Performance $DeNO_x$ Catalysts Based on $Mn_xCo_3-_xO_4$ Nanocages Derived from Metal−Organic Frameworks. *ACS Catal.* **2014**, *4*, 1753−1763.
(37) Mohanty, J.; Barooah, N.; Dhamodharan, V.; Harikrishna, S.; Pradeepkumar, P. I.; Bhasikuttan, A. C. Thioflavin T as an efficient inducer and selective fluorescent sensor for the human telomeric G-quadruplex DNA. *J. Am. Chem. Soc.* **2013**, *135*, 367−376.
(38) Sigel, R. K. O.; Sigel, H. stability concept for metal ion coordination to single-stranded nucleic acids and affinities of individual sites. *Acc. Chem. Res.* **2010**, *43*, 974−984.
(39) Bai, Y.; Zhao, L.; Chen, Z.; Wang, H.; Feng, F. A label-free fluorescent sensor for Pb^{2+} based on GQ and graphene oxide. *Anal. Methods* **2014**, *6*, 8120−8123.
(40) Fu, T.; Ren, S.; Gong, L.; Meng, H.; Cui, L.; Kong, R. M.; Zhang, X. B.; Tan, W. A label-free DNAzyme fluorescence biosensor for amplified detection of Pb^{2+}-based on cleavage-induced GQ formation. *Talanta* **2016**, *147*, 302−306.
(41) Zhang, B.; Wei, C. Highly sensitive and selective detection of Pb^{2+} using a turn-on fluorescent aptamer DNA silver nanoclusters sensor. *Talanta* **2018**, *182*, 125−130.

https://dx.doi.org/10.1021/acsomega.0c03257
ACS Omega XXXX, XXX, XXX−XXX

(42) Kim, J. H.; Han, S. H.; Chung, B. H. Improving Pb^{2+} detection using DNAzyme-based fluorescence sensors by pairing fluorescence donors with gold nanoparticles. *Biosens. Bioelectron.* **2011**, *26*, 2125−2129.
(43) Liang, H.; Xie, S.; Cui, L.; Wu, C.; Zhang, X. Designing a biostable L-DNAzyme for lead (II) ion detection in practical samples. *Anal. Methods* **2016**, *8*, 7260−7264.
(44) Peng, D.; Li, Y.; Huang, Z.; Liang, R. P.; Qiu, J. D.; Liu, J. Efficient DNA-catalyzed porphyrin metalation for fluorescent ratiometric Pb^{2+} detection. *Anal. Chem.* **2019**, *91*, 11403−11408.
(45) Chen, M.; Hassan, M.; Li, H.; Chen, Q. Fluorometric determination of lead (II) by using aptamer-functionalized upconversion nanoparticles and magnetite-modified gold nanoparticles. *Microchim. Acta* **2020**, *187*, 1−9.
(46) Zhou, W.; Ding, J.; Liu, J. 2-Aminopurine-modified DNA homopolymers for robust and sensitive detection of mercury and silver. *Biosens. Bioelectron.* **2017**, *87*, 171−177.
(47) Pu, W.; Zhao, H.; Huang, C.; Wu, L.; Xua, D. Fluorescent detection of silver (I) and cysteine using SYBR Green I and a silver (I)-specific oligonucleotide. *Microchim. Acta* **2012**, *177*, 137−144.
(48) Wang, Z.; Xiao, X.; Yang, Y.; Zou, T.; Xing, X.; Zhao, R.; Wang, Z.; Wang, Y. L-Aspartic Acid Capped CdS Quantum Dots as a High Performance Fluorescence Assay for Sliver Ions (I) Detection. *Nanomaterials* **2019**, *9*, 1165.
(49) Qi, L.; Yan, Z.; Huo, Y.; Hai, X. M.; Zhang, Z. Q. MnO_2 nanosheet-assisted ligand-DNA interaction-based fluorescence polarization biosensor for the detection of Ag^+ ions. *Biosens. Bioelectron.* **2017**, *87*, 566−571.
(50) Hu, L.; Zhang, P.; Chen, Q. W.; Yan, N.; Mei, J. Y. Prussian Blue Analogue $Mn_3[Co(CN)_6]2.nH_2O$ porous nanocubes: large-scale synthesis and their CO_2 storage properties. *Dalton Trans.* **2011**, *40*, 5557−5562.
(51) Wang, D.; Wu, H.; Zhou, J.; Xu, P.; Wang, C.; Shi, R.; Wang, H.; Wang, H.; Guo, Z.; Chen, Q. In Situ One-Pot Synthesis of MOF−Polydopamine Hybrid Nanogels with Enhanced Photothermal Effect for Targeted Cancer Therapy. *Adv. Sci.* **2018**, *5*, 1800287.

https://dx.doi.org/10.1021/acsomega.0c03257
ACS Omega XXXX, XXX, XXX−XXX